
Article:
Carey, John Joseph and McKenna, Keith Patrick orcid.org/0000-0003-0975-3626 (2019) Screening Doping Strategies to Mitigate Electron Trapping at Anatase TiO2 Surfaces. Journal of Physical Chemistry C. ISSN 1932-7455

https://doi.org/10.1021/acs.jpcc.9b05840

Screening Doping Strategies to Mitigate Electron Trapping at Anatase TiO_2 Surfaces

John J. Carey* and Keith P. McKenna*

Department of Physics,University of York, Heslington, YO10 5DD, York, United Kingdom

E-mail: john.carey@york.ac.uk; keith.mckenna@york.ac.uk

Abstract

Nanocrystalline anatase titanium dioxide is an efficient electron transport material for solar cells and photocatalysts. However, low coordinated Ti cations at surfaces introduce low lying Ti $3d$ states that can trap electrons, reducing charge mobility. Here, a number of dopants (V, Sb, Sn, Zr, Hf) are examined to replace these low coordinated Ti cations and reduce electron trapping in anatase crystals. V, Sb and Sn dopants act as electron traps, while Zr and Hf dopants are found to prevent electron trapping. We also show alkali metal dopants can be used to fill surface traps by donating electrons into the $3d$ states of low coordinated Ti ions. These results provide practical guidance on the optimization of charge mobility in nanocrystalline TiO_2 by doping.

Introduction

Titanium dioxide (TiO_2) is an important and widely used semiconductor and photocatalyst,[1–7] which is extremely useful for a range of applications including, dye sensitized solar cells,[8,9] water splitting,[10–12] pollution abatement,[13,14] and CO_2 reduction.[15–17] The inexpensiveness, abundance, and superior electron transport properties of TiO_2 make it appealing for

these applications.[18–20] There are a number of TiO_2 polymorphs that have different electronic transport properties, while the rutile phase is the most thermodynamically stable phase, the anatase phase (a-TiO_2) is the more catalytically active material, and most studied.[21–24] In solar energy applications, a-TiO_2 is used as a transport material where the electron mobility is critical to the performance of the device, whereas for water splitting a-TiO_2 is irradiated with light, generating electron-hole separated charge carriers.[2,25] The transport of electrons (e^-) and holes (h^+) for both applications is vital to the efficiency of a-TiO_2, where facet dependent migration from bulk a-TiO_2 to the surfaces can occur.[26,27] Ideally for water splitting separation of electrons and holes is required, however charge recombination and annihilation can occur which is detrimental to conductivity.[26,28–31] The charge carriers can also localize on native cation/anion lattice sites (self-trapping) at surfaces, defects, dislocations, interfaces or indeed within the bulk material, affecting their mobility throughout TiO_2, which greatly affects its performance as an electron transport material for energy applications.

The self-trapping of electron and hole charge carriers in anatase TiO_2 affects electron transport, charge recombination rates and overall device efficiency. Shallow traps lie close to the conduction or valence band edges and mediate transport in TiO_2,[32] while deeper traps in the band gap promote carrier recombination.[33] Electrochemical and photoluminescence studies provide valuable insights into the nature of traps in metal oxide samples.[34–37] There is no direct evidence to suggest that electron trapping occurs in bulk a-TiO_2, but electron trapping does occur at surfaces of anatase TiO_2.[37–39] Surface trapped electrons have first order steady state kinetics with slow hopping from trap to trap.[36] The surface states associated with trapped electrons have a distinct Fermi level from that of the bulk material, which leads to a non-uniform Boltzmann distribution resulting in barriers to detrapping.[39] The nature of the electron traps on different exposed surfaces of nano-crystalline anatase TiO_2 remains unclear, where the trapping of the photogenerated electrons, and their hole counterparts, is facet dependant with their spatial separation, distribution and density of traps on specific facets playing a key role.[26,29,34–36] Indeed the trapping of electrons at different surface facets

are found to interact differently with adsorbates, such as O_2 and H_2O, facilitating different reaction mechanisms to suggest that the affinity to trap electrons influences the facet reactivity and charge transfer.[38–40]

The focus of this paper is build on previous work examining electron trapping at the anatase surfaces, and identify suitable dopants than can either remove or nullify electron traps on nano-crystalline a-TiO_2. Experimental studies investigating electron trapping have alluded to surface traps being present on nano-crystalline anatase TiO_2 from two sources; oxygen vacancy formation, and/or low coordinated Ti cations on the surface.[37,41,42] Our recent work using hybrid density functional theory (DFT) calculations have shown that electron trapping does not occur in the bulk of anatase TiO_2,[43] and further calculations showed that there were no electron trapping surface states on the defect free, pristine low index surfaces,[44] however using the a-TiO_2 (103) stepped surface as an example, we showed that low coordinated Ti cations contributed to electron trapping. Our work is in agreement with DFT calculations using a Hubbard +U (DFT+U) correction which have modelled the behaviour of excess electrons in TiO_2 showing that a carrier free description of electrons occupying conduction band states (i.e. no electron trapping) is accurate,[45] but in contrast to other previous DFT+U work.[46–50] Our calculations challenge the convention that low index pristine surfaces contain electron trap states on facets of a-TiO_2, and suggest that undercoordinated Ti cations from surface defects are a more stronger contributing factor than point defects for electron trapping. These low coordinated Ti cations introduce defect states lying at the bottom of the conduction band that can trap excess electrons, but do not generate any additional electrons in the system,[44,51–54] whereas point defects such as oxygen vacancies introduce filled defective states that cannot trap additional electrons.[50,55–58]

In the present study hybrid DFT calculations are used to investigate substitutional doping of the low coordinated Ti cations on a-TiO_2, and show that they can remove the surface states at the bottom of the conduction band associated with electron trapping. In our previous work, electron trapping occurs on the (103) surface and this is used as a model to

demonstrate that doping can remove electron traps. Typically doping in a-TiO_2 is carried out to improve the TiO_2 as a photocatalyst various chemical modifications to change the electronic structure for TiO_2 to adsorb in the visible light spectrum. Some examples of improving the photoconductivity of TiO_2 in such a way include nitrogen,[59–63] transition metal,[64,65] sulphur,[66–68] carbon,[69,70] boron,[71] lanthanide,[72] zirconium,[73–75] and flourine.[76] Although many doping studies in the literature are focused on altering the band gap of TiO_2 for photocatalysis, there have been few that specifically examine the influence dopants have on electron traps in anatase TiO_2 nanocrystals. Our focus therefore is to go beyond the conventional thinking of doping TiO_2 by this approach, and examine candidates on the (103) surface that will remove electron traps. We find that dopants such as V, Sb and Sn trap additional electrons similar to Ti, while Zr and Hf species do not trap excess electrons and we show why these species are suitable candidates to remove electron traps. We also demonstrate that electron donating alkali metals (Li, Na, K, Rb, Cs) can fill the surface traps, and are another approach to remove electron traps from a-TiO_2

Computational Methodology

Hybrid density functional theory (DFT) calculations using the generalized gradient approximation (GGA) were carried out using the CP2K simulation package.[77] Exact Hartree-Fock (HF) exchange is mixed into the exchange-correlation functional (hybrid-DFT) to overcome the issue of the self-interaction error (SIE) that is well known in DFT. We use a truncated PBE0 hybrid-DFT exchange-correlation functional that includes long range corrections to the interaction potential (PBE0-TR-LRC) with a global $\frac{1}{r}$ dependence. This defines a range of separations in the electron integrals to implement the HF exact exchange, and standard PBE is used outside of this defined range. The truncation radius (R_c) must be smaller than half the distance of the lattice vectors to ensure that there is no interaction between neighbouring cells, and we set our radius to 6.00 Å shown previously to give converged structural

and electrical properties.[43] The percentage of HF exact exchange to include in these calculations was parameterized by satisfying Koopmans' condition to within 0.05 eV for electron and hole polarons in bulk TiO_2 anatase (yielding $\alpha = 10.5\%$) which gives a band gap within 3% of the experimental value.[43] Triple ζ basis sets were used for both titanium and oxygen for accurate calculations,[78,79] and the Goedecker-Teter-Hutter (GTH) pseudopotentials for both species available within CP2K.[80–82] A multi-grid approach for mapping products of Gaussians onto a real-space integration grid is used in CP2K, where the wide and smooth Gaussian functions are mapped onto a coarser grid, and the electron density is mapped onto the finest grid. The plane wave energy cut-off, a reference grid which controls the Gaussian mapping onto the multi-grid, is set to 60 Ry. Five multi-grids are used, and the plane wave cut-off is sufficiently converged at 600 Ry for the finest level of the multi-grid. The electronic properties of the electron trapped in each surface will be detailed by spin density, partial (l quantum number decomposed) electronic density of states (PEDOS). The number of electrons for each species is determined using Bader's atoms in molecules (AIM) approach,[83] implemented by Henkelman *et al.*.[84–87] All structural images and spin density plots are visualised using the VESTA software.[88,89] Further details on our computational method and set-up are detailed in the Supporting Information.

Results

The optimized (103) surface is shown in Fig. 1. The (103) surface is terminated with four coordinated Ti cations (Ti_{surf}) and two coordinated O anions, while the sub-surface layers have six coordinated Ti cations (Ti_{sub}) and three coordinated O anions similar to bulk anatase TiO_2. Surface Ti_{surf} cations and O anions have bond lengths ranging from 1.69Å to 1.98Å. The Ti cations in the bulk region of the slab (Ti_{bulk}) have similar bond lengths (<1% deviation) to the optimized anatase TiO_2 bulk, and can be used as a reliable reference for calculating electron trapping energies. The partial decomposed (species and

angular momentum) electronic density of states (PEDOS) plots for Ti cations in different environments in the surface slab are also shown in Fig. 1. The band gap for both the surface and bulk regions is 3.12 eV, and in good agreement (<3%) of the experimental band gap (3.2 eV). The most noticeable difference between the Ti_{surf} and Ti_{bulk} cations, is the large Ti $3d$ peak at the bottom of the conduction band (CBM) associated with the Ti_{surf} cations that is absent for Ti_{bulk} cations. The presence of states associated with the Ti_{surf} cations at the CBM will have implications for electron trapping in the (103) surface of anatase TiO_2. The calculated Bader charge for the Ti_{surf} ions is 9.8 electrons (e^-) or a charge of +2.2 since our Ti potential contains 12 valence electrons. For Ti_{sub} and Ti_{bulk} the Bader charge is 9.7 e^- (+2.3), and the O surface anions have a charge of 7.2 e^- or -1.2 since there are 6 valence electrons in the potential. Both Ti cations and O anions have a spin of 0.0 μ_β.

As shown from our previous work,[44] the only site capable of trapping an excess electron is the Ti_{surf} cation, as shown in Fig. 1 (b), while all other sites in the sub surface and bulk regions prefer delocalised electronic solutions similar to bulk a-TiO_2.[43] The electron trapped at this site reduces Ti^{4+} to Ti^{3+} as we see a decrease in the Ti_{surf} charge from +2.2 to +2.0, which some further charge spread across neighbouring ions. The presence of the trapped electron increases the spin on the Ti cation from 0.0 to 0.74 μ_β. The geometric structure around the reduced Ti cation becomes distorted with surface bond lengths increasing by 0.1 - 0.15Å . The calculated trapping energy is +0.07 eV with respect to the delocalised solution in the bulk of the slab implying that electrons would prefer to be delocalised in the bulk crystal than trapped at low coordinated surface Ti atoms. The trapping of electrons at these sites can be considered to be kinetically trapped, as observed by experiment,[36] but being thermodynamically unfavourable. The PEDOS shows that the electron trap is a shallow donor, where the occupied Ti $3d$ defect peak is 0.45 eV below the CBM. This peak was previously seen at the conduction band edge (Fig. 1 (a)) and the trapped electron fills this state.

The dopants we initially consider to passivate the Ti_{surf} electron trap are V, Sb, Sn, Zr

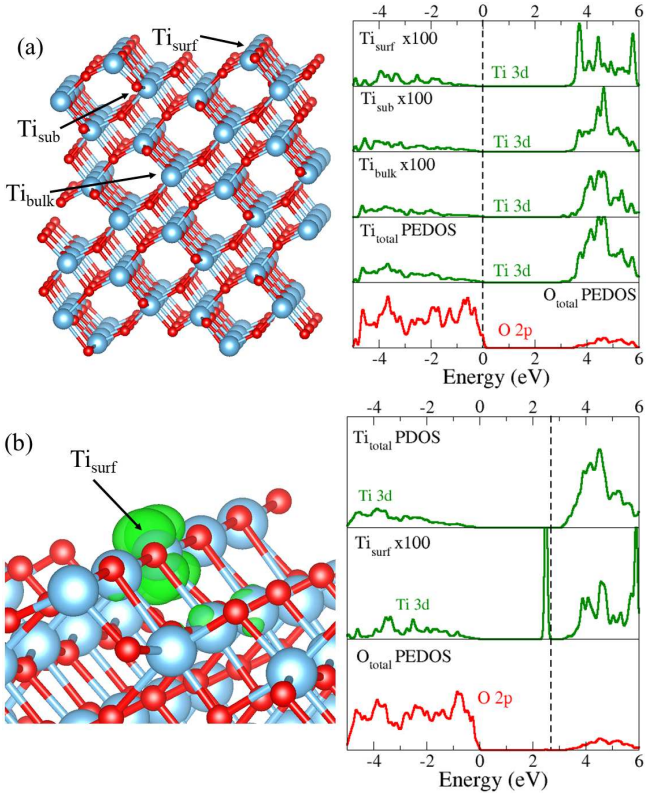

Figure 1: (a) The (103) surface slab and calculated PEDOS for different Ti cations, and (b) the local geometry of an electron trapped at a surface Ti atom and the associated PEDOS. The blue and red spheres are the lattice sites for the Ti cations and O anions, while the green and red lines are the Ti $3d$ and O $2p$ projected DOS.

and Hf (that all have a stable +4 oxidation state). Zr and Hf are of particular interest as these species are known to be polaronic materials in their parent MO_2 oxides.[90–93] These materials have contrasting polaronic behaviour, only hole trapping is seen in ZrO_2 while both electron, and hole trapping is observed in HfO_2. This will allow a comparison between with each other and other dopant species for examining their behaviour and effect on electron trapping in TiO_2. The dopants can replace the low coordinated Ti cations on the surface, where the rationale is to remove the states at the CBM associated with electron trapping (Fig. 1). The distribution of dopants were examined in different layers of the slab from the surface (1) to the bulk region (4) as shown in Fig. 2, where the calculated relative energies for each layer are given in Table 1. We find that there is a difference of around 0.2 eV between the different surface and sub-surface sites, suggesting that the dopants could potentially replace either the four or six coordinated Ti cations. In the bulk region of the slab, Sn, Zr and Hf have more favoured energies compared to the surface region, however, although the thermodynamics may suggest that they are more stable there would be a large experimental kinetic barrier to drive these dopants into a bulk region to replace Ti cations in TiO_2 nano-crystals, and thus the dopants would be expect to be in the surface region. For the interest of this study we will focus on replacing the Ti_{surf} cations.

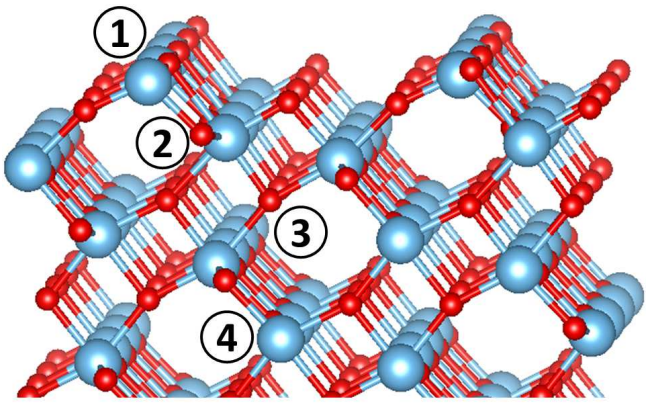

Figure 2: The different lattice positions in the surface slab examined for the dopant distribution.

After relaxation, all the dopants maintain the same geometry and coordination of the

Table 1: The calculated energies relative to the surface site for the distribution of dopants in the (103) slab as shown in Fig. 2.

Bond	1 (eV)	2 (eV)	3 (eV)	4 (eV)
V	0.00	+0.11	+0.32	+0.32
Sb	0.00	+0.21	+0.55	+0.55
Sn	0.00	-0.09	-0.54	-0.46
Zr	0.00	-0.11	-0.49	-0.29
Hf	0.00	-0.19	-0.44	-0.34

Ti cation site with changes to the bond lengths. The calculated metal-oxygen bond lengths in the surface layer (M-O_{surf}), and the sub-surface layer (M-O_{sub}) are given in Table 2. All dopants have longer bond lengths than Ti-O, with the largest change seen for the bonds oriented towards the sub surface layer, where Sb and Zr show the greatest increase. The dopants distort the local geometry on the surface, with changes in Ti-O bond lengths being observed to the next nearest neighbour positions.

Table 2: The calculated bond lengths for the Ti-O surface bonds and the dopant-O bonds.

Bond	M-O_{surf} (Å)	M-O_{sub} (Å)
Ti-O	1.98 (x2)	1.83, 1.69
V-O	2.01 (x2)	1.82, 1.61
Sb-O	2.15 (x2)	1.99, 1.89
Sn-O	2.05 (x2)	1.98, 1.89
Zr-O	2.10 (x2)	1.96, 1.84
Hf-O	2.06 (x2)	1.92, 1.83

The calculated partial density of states (PDOS) for each of the doped surfaces are shown in Fig. 3. There are significant differences in the electronic structure for the V and Sb dopants when replacing a Ti_{surf} ion. The V dopant has a +4 oxidation state with one unpaired electron as shown by the occupied V $3d$ peak around 1 eV above the VBM, and has a spin of $0.97\,\mu_\beta$. Sb can adopt a +4 oxidation state in one phase of its parent oxides,[94] and the Sb dopant has a +4 oxidation state when replacing the Ti cation with an unoccupied Sb $5p$ state around 1 eV above the VBM (Fig. 3 (c)) and a spin of $0.36\,\mu_\beta$, thus behaving in a similar manner to Sb doping of SnO_2.[95,96] The potentials for V and Sb have 13 and 5 electrons respectively, so using the calculated Bader values for the V and Sb dopants their

charges are +2 and +3.8 respectively. The Sb dopant has a larger charge than either Ti or V. Further inspection of the Bader charges and volumes shows that due to the larger ionic radius of Sb some of the charge on Sb is incorrectly assigned to the surrounding oxygen atoms. Accounting for this fact, the real Sb Bader charge is found to be around +2.2. The Sn, Zr and Hf dopants have a +4 oxidation state similar to the Ti^{+4} cation, and do not introduce any defect states in the band gap (Fig. 3 (c), (e), (f)), where their absence shows that these dopants are isoelectronic to Ti. The charges for Sn, Zr and Hf dopants are +4.0, +2.5 and +2.6. Similar to Sb, the Bader charge on the Sn ion is misleading due to its large ionic radius. Accounting for the charge on the surrounding oxygen atoms the Sn dopant has a charge of +2.4. All dopants have a spin of 0.0 μ_β.

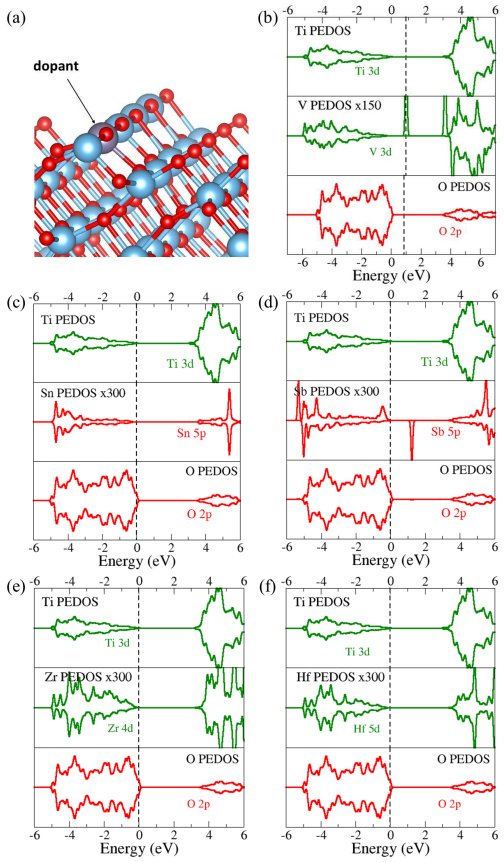

Figure 3: (a) The local structure of the (103) surface and the calculated PEDOS plots for (b) V, (c) Sn, (d) Sb, (e) Zr and (f) Hf doped surfaces. The blue and red spheres are the Ti and O ions, while the red and green lines are the p and d states.

In order to examine the electron trapping behaviour of these dopants, an additional

electron is added in the presence of a precursor polaronic distortion around the Ti_{surf} site and optimized self consistently. The lowest energy configurations of the excess electron for each dopant species are shown in Fig. 4. The addition of an electron to the V doped surface leads to reduction of the V dopant (V^{4+} to V^{3+}). The added electron becomes spin paired with the previous unpaired electron on the V ion. There is an decrease in the charge of the V ion from +2.0 to +1.7 resulting in a spin of -0.03 μ_β. The reduction of the V ion is 0.13 eV more favourable than the delocalised solution in the bulk, and 0.22 eV more favourabale than trapping at other Ti_{surf} cations. A similar behaviour is seen for the Sn doped surface when an electron is added. The electron preferentially traps on the Sn dopant in the a-TiO_2 (103) surface over the Ti_{surf} cations as shown by the spin density plot in Fig. 4 (b), with a calculated trapping energy of -0.01 eV compared to the delocalised solution in the bulk, and 0.01 eV more favoured than an electron trapped on a nearby Ti_{surf} cation. There is a decrease in charge of the Sn dopant from +2.4 to +1.7 and an increase in spin to 0.6 μ_β indicating a reduction of Sn^{+4} to Sn^{+3}. For the Sb doped surface, the addition of an electron fills the unoccupied Sb $5p$ state on the Sb dopant. Reduction of surface Ti cations near the Sb dopant was not energetically feasible and the electron always favoured migrating to fill the unoccupied Sb $5p$ state on the Sb dopant. The charge decreases from +2.2 to +1.4, and the spin decreases to 0.0 μ_β confirming the reduction of the Sb dopant. The calculated energy to fill the unoccupied defect state is -0.001 eV compared to the delocalised solution in the bulk indicating that the excess electron has no preference between the Sb dopant and bulk. When an excess electron is trapped at the Ti_{surf} cation beside a dopant species, it will migrate under surface relaxation onto a dopant cation indicating that electrons are more likely to be present on the dopant than the Ti_{surf} cation suggesting these dopants act as stronger trapping sites than surface Ti_{surf} cations.

A different electron trapping behaviour is observed for the Zr and Hf doped (103) a-TiO_2 surfaces. An additional electron will not localise on the the Zr or Hf dopant as seen for V, Sn, and Sb, and the electron preferentially migrates to reduce another Ti_{surf} cation as shown

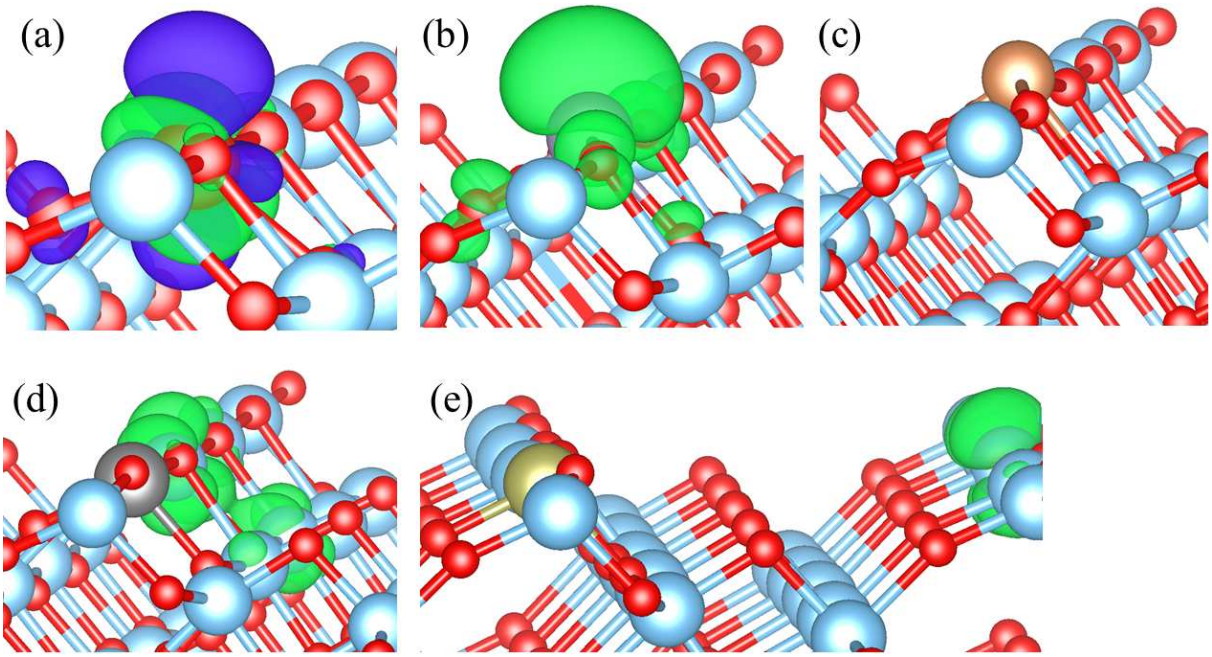

Figure 4: The local geometry, spin density plot for electron trapping in (a) V, (b) Sn, (c) Sb, (d) Zr and (e) Hf doped (103) surface slab. The blue and red spheres are the lattice sites for the Ti cations and O anions, while the green iso-surface shows the location of the excess electron (0.004 electrons/Å^3).

in Fig. 4 (d) and (e). This occurs on next nearest neighbour sites for Zr doped surface, while for Hf doped TiO_2 the electron will migrate to the next chain of Ti_{surf} cations. The reduced Ti cation has an decrease in charge from +2.2 to +1.9. It was still energetically unfavourable to localise an electron on the dopant using 25% HF exchange, and the electron migrated to a low coordinated surface Ti, suggesting that electron trapping will never occur on the Zr and Hf dopants. Trapping the electron on the doped Zr and Hf surfaces costs an energy of +0.17 eV and +0.10 eV, respectively, relative to a delocalised electron in the anatase bulk indicating that the presence of the dopant makes it less favourable for the electron to be present at the surface. These dopant species do not trap electrons as there are no low energy peaks at the CBM capable of accomodating extra electrons as shown by the PEDOS plots.

The calculated PEDOS plots given in Fig. 5 provide further evidence to the electron trapping nature of the V, Sn and Sb dopants, while showing that no trapping occurs on Zr and Hf dopants. The reduction of V and Sn dopants by trapping an excess electron is shown

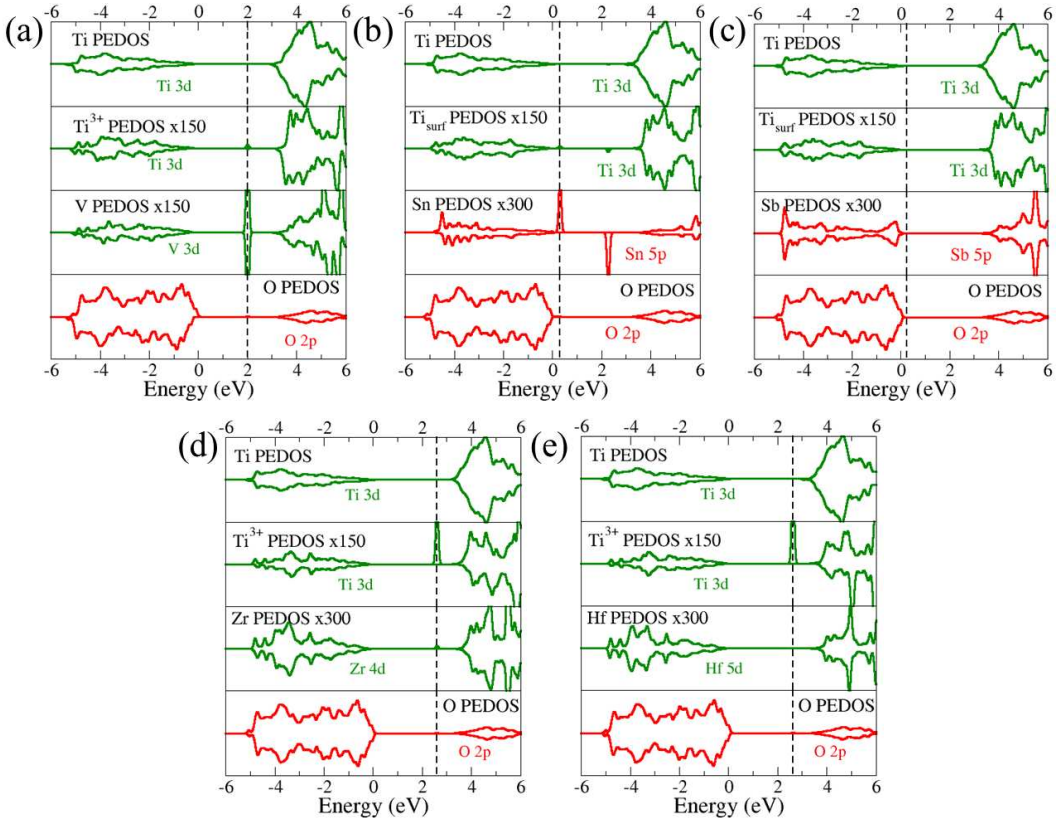

Figure 5: The calculated PEDOS plot for electron trapping in (a) V, (b) Sn, (c) Sb, (d) Zr and (e) Hf doped (103) surface slab. The red and green lines are the p and d states.

by the defect levels in the band gaps (Fig. 5 (a) and (b), where the excess electron on V pairs with the previous unpaired electron (Fig. 3 (b)) having a deep defect level around 1 eV below the CBM, while for Sn the extra electron occupies a Sn $5p$ defect level 0.25 eV above the VBM. The presence of a Sn $5p$ defect level at the CBM suggests that further electron trapping is likely on the Sn dopant. The absence of a defect peak in the band gap for the Sb doped surface supports the filling of the unoccupied defect state by the excess electron. For the Zn and Hf dopants, the shallow defect Ti $3d$ level around 0.45 eV below the CBM is an indication of electron trapping on the Ti_{surf} cations. Trapping does not occur on the dopants as their d band states lie deep in the CB and a wider number of states near the CBM is similar to bulk TiO_2 suggesting that no electron trapping can occur.

Another approach to reduce electron trapping in anatase TiO_2 is the introduction of electron donating species to fill the electron surface traps. In order to examine this, we introduced alkali metal (Li, Na, K, Rb, Cs) interstitials into the anatase (103) surface. Alkali metal doped TiO_2 is well studied, especially Li doped TiO_2, where many experimental studies have shown that alkali metal can easily be incorporated into TiO_2 and show improvements in conductivity over undoped TiO_2.[97–100] Their effect however on electron traps in TiO_2 has not been considered, and is an interesting approach to consider to nullify the electron traps that exist on anatase TiO_2 crystals. In order to find the most energetically favoured interstitial position, the metal ions were relaxed in various sites in the surface and sub-surface layers with the relaxed geometry for the lowest energy position of each species shown in Fig. 6. There appears to be an ionic radius size effect on the lowest energy configuration. The smaller Li and Na ions reside in the subsurface layers, while the larger K, Rb and Cs ions prefer to move from the sub surface layers and sit on the (103) surface. Rb and Cs interstitials are large enough to form additional Rb/Cs-O bonds with the O anions in the step pulling them away from the coordinated Ti cations, resulting in the Ti cation becoming three coordinated. The calculated bond lengths for the alkali interstitials in the (103) surface are given in Table 3, where the increase in bond lengths with increasing ionic radius can be seen. The bond

lengths for the large cations becomes too large for the surface to accommodate the interstitial so K/Rb/Cs migrate to the surface edge in order to relieve any surface strains.

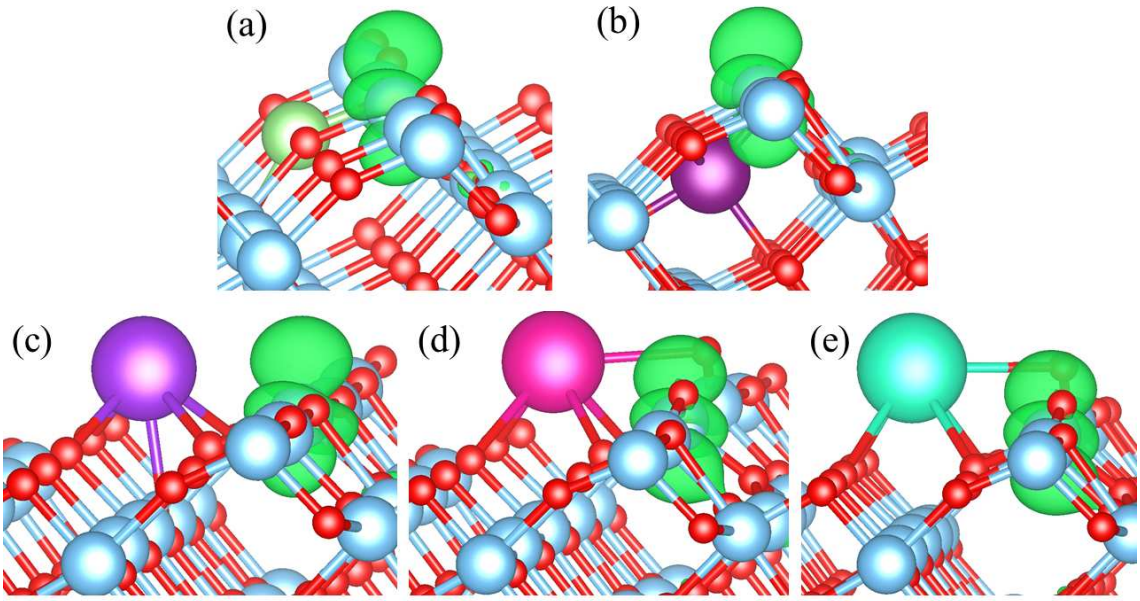

Figure 6: The local geometry of the alkali metal interstitials in the (103) surface slab for (a) Li, (b) Na, (c) K, (d) Rb and (e) Cs. The blue and red spheres are the lattice sites for the Ti cations and O anions, while the green, purple, magenta, pink and turquoise spheres are the Li, Na, K, Rb and Cs interstitials. The position of the excess electron is shown by the green spin density plot (0.004 electrons/Å^3).

Table 3: The calculated bond lengths for the metal-oxygen surface bonds of the interstitial ions along the a and c directions.

Bond	a direction (Å)	c direction (Å)
Li-O	1.90 (x2)	2.12, 1.95
Na-O	2.18 (x2)	2.22, 2.14 (x2)
K-O	2.62 (x2), 2.79 (x2)	3.10
Rb-O	3.00	2.90 (x4)
Cs-O	3.06	3.10 (x4)

The spin density plots in Fig. 6 show that the neighbouring Ti_{surf} cation contains excess electron density donated from the presence of the alkali metal interstitial ion. The alkali metal donates the electron to fill the electron trap state that resides at the bottom of the CBM, reducing the Ti^{+4} to Ti^{+3}. This electron donating process is supported by the calculated PEDOS plots for Li and Na incorporation in TiO_2 as shown in Fig. 7, where

only the plots for Li and Na interstitials are shown since the PEDOS plots for the other alkali metals have similar characteristics. There are negligible Li/Na 1/2 s states in the VB suggesting that a small amount of electron occupation resides on the alkali metal, while the occupation of the electron trap is seen with the presence of the defect peak around 1 eV from the CBM on the Ti PEDOS. The reduction process for each surface is also supported by the decrease in the Ti_{surf} cation charge from +2.2 to +1.9, and an increase in the spin on the reduced Ti cation from 0.0 to 0.88 μ_β.

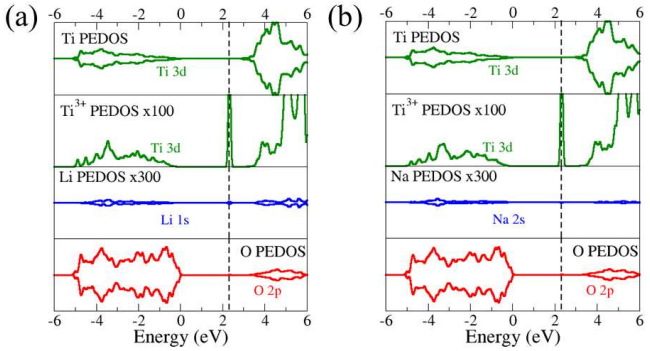

Figure 7: The calculated PEDOS plots for (a) Li, and (b) Na doped TiO_2. The blue, red and green lines are the s, p, and d states, where the black dotted line shows the position of the fermi level. The top of the valence band is aligned to 0 eV.

Discussion

Electron self trapping is harmful to the performance of TiO_2 as an electron transport layer in solar cell devices since the excess electrons from an external bias will trap at Ti cation lattice sites reducing its efficiency. Reducing or removing these traps from TiO_2 nano-composites is of critical importance to ensure that electrons are allow to flow through the medium without hindrance. We examined two approaches to reduce the contribution of low coordinated surface Ti cations towards electron trapping in nano-crystals of anatase TiO_2; (1) substitutional doping to remove the Ti $3d$ states associated with electron traps, and (2) introduction of electron donating interstitials to fill the associated Ti $3d$ electron trap states. The examined dopants with stable variable oxidation states such as V and Sb were found

not to relieve electron trapping at the (103) surface. V introduced more electron traps to the system as low lying V d states were introduced at the CBM, and could be further reduced from V^{+4} to V^{+3}. It is also more energetically favoured to carry out this reduction than having electrons delocalised in the bulk system. The Sb dopant is also not a good candidate to reduce electron trapping in the (103) surface as this dopant introduces unoccupied defect states into the surface. These states act as electron traps in addition to the low coordinated Ti cations. We also found that using Sn as a dopant to reduce electron trapping was not viable as it was more favoured to reduce the Sn dopant than the Ti cations. Sn is more electronegative than Ti and will have a tendancy to attract electrons, while the lower lying Sn $5p$ states in the conduction band are more easily accessed than the Ti $3d$ states. From our predictions it is therefore not advisable to use V, Sn or Sb as chemical modifications in a-TiO_2 for solar cell applications as these species further contribute to electron trapping. The migration of Sn ions into a-TiO_2 when examining a SnO_2/TiO_2 composite,[101,102] can greatly affect the electron transport efficiency since Sn will trap electrons, and thus preventing Sn incorporation in a-TiO_2 is desirable to maintain the photocatalytic activity and electron transport properties.

Both Zr and Hf were found to be useful candidates to remove electron traps from the (103) surface of anatase TiO_2. These dopants removed the trapping states at the CBM associated with electron trapping, as the Zr $4d$ and Hf $5d$ states are higher in energy. The additional electrons could not localise on the Zr/Hf because of this, and it was more energetically favourable to move to and reduce the low coordinated Ti cations. Increasing the concentration of these dopants could eliminate more of the Ti_{surf} electron traps leading to improved mobility in a-TiO_2. Using non-reducible dopants such as Zr is beneficial to reduce electron trapping in anatase TiO_2 since this species removes low lying electron trapping states at the CBM. Experimental studies have eluded to Zr doping improving photocatalytic properties of a-TiO_2, and doping with Zr to remove electron traps is a perhaps a contributing factor to this improvement.[103–106]

The use of alkali metal candidates is also useful for removing electron traps from anatase TiO_2. These species donated electrons into the low coordinated Ti cations and filled the electron trap states at the CBM. Any additional electrons into the anatase crystals would therefore not get trapped since the states are now filled. Using electron donating species is beneficial to reduce electron trapping in anatase TiO_2.

Conclusion

In summary, hybrid-density functional theory was used to examine approaches to reduce electron trapping in nano-crystals of TiO_2. Low coordinated Ti cations on surfaces of anatase TiO_2 were found to greatly contribute to electron trapping since these species introduce low lying Ti $3d$ states at the bottom of the conduction band. These states can then be filled with additional electrons in the nano-crystal and the electrons become trapped at these surface artifacts. A number of dopants were examined to replace these low coordinated Ti cations and reduce electron trapping in anatase TiO_2. Dopants such as V and Sb that can achieve stable variable oxidation states were found to enhance electron trapping through the introduction of additional defect states in the band gap or the bottom of the conduction band. This is expected to reduce electron mobility in anatase TiO_2 as these dopants would act as electron traps in addition to the low coordinated surface Ti cations. We found that Zr and Hf will improve electron mobility in anatase TiO_2 as these species do not introduce additional defect peaks or further d state peak traps at the bottom of the conduction band, reducing the number of electron traps present in samples. Alkali metals are also expected to improve electron transport in TiO_2. These species can donate extra electrons into the low lying Ti $3d$ states at the bottom of the conduction band associated with electron trapping. If the traps are already filled by these alkali earth metal interstitials then additional electrons into nano-crystals of anatase TiO_2 are expected not to trap and thus reducing electron trapping.

Supporting Information Available

Supporting Information Available: Further computational details and set up.

This material is available free of charge via the Internet at `http://pubs.acs.org/`.

Acknowledgement

K.P.M. and J.J.C acknowledge support from EPSRC (EP/K003151/1, EP/P006051/1 and EP/P023843/1). This work made use of the facilities of Archer, the UK's national high-performance computing service, via our membership in the UK HPC Materials Chemistry Consortium, which is funded by EPSRC (EP/L000202/1). This work also made use of the facilities of N8 HPC Centre of Excellence, provided and funded by the N8 consortium and EPSRC (EP/K000225/1). The Centre is coordinated by the Universities of Leeds and Manchester. Work on this project also made use of the Viking Cluster, which is a high performance compute facility provided by the University of York. All data created during this research are available by request from the University of York Research database (https://pure.york.ac.uk/portal/en/).

References

(1) Gordon, T. R.; Cargnello, M.; Paik, T.; Mangolini, F.; Weber, R.; Fornasiero, P.; Murray, C. Nonaqueous Synthesis of TiO_2 Nanocrystals Using TiF_4 to Engineer Morphology, Oxygen Vacancy Concentration, and Photocatalytic Activity. *Journal of the American Chemical Society* **2012**, *134*, 6751–6761.

(2) Jian, P.; Gang, L.; Qing, L. G.; Hui-Ming, C. On the True Photoreactivity Order of {001}, {010}, and {101} Facets of Anatase TiO_2 Crystals. *Angewandte Chemie International Edition* **2011**, *50*, 2133–2137.

(3) Zheng, Z.; Huang, B.; Lu, J.; Qin, X.; Zhang, X.; Dai, Y. Hierarchical TiO_2 Microspheres: Synergetic Effect of {001} and {101} Facets for Enhanced Photocatalytic Activity. *Chemistry A European Journal* **2011**, *17*, 15032–15038.

(4) Wang, Z.; Huang, B.; Dai, Y.; Liu, Y.; Zhang, X.; Qin, X.; Wang, J.; Zheng, Z.; Cheng, H. Crystal Facets Controlled Synthesis of Graphene at TiO_2 Nanocomposites by a One-pot Hydrothermal Process. *CrystEngComm* **2012**, *14*, 1687–1692.

(5) Yang, H. G.; Sun, C. H.; Qiao, S. Z.; Zou, J.; Liu, G.; Smith, S. C.; Cheng, H. M.; Lu, G. Q. Anatase TiO_2 Single Crystals with a Large Percentage of Reactive Facets. *Nature* **2008**, *453*, 638–641.

(6) Etgar, L.; Zhang, W.; Gabriel, S.; Hickey, S. G.; Nazeeruddin, M. K.; Eychmüller, A.; Liu, B.; Grätzel, M. High Efficiency Quantum Dot Heterojunction Solar Cell Using Anatase (001) TiO_2 Nanosheets. *Advanced Materials* **2012**, *24*, 2202–2206.

(7) Nolan, M.; IwaszuK, A.; Lucid, A. K.; Carey, J. J.; Fronzi, M. Design of Novel Visible Light Active Photocatalyst Materials: Surface Modified TiO_2. *Advanced Materials* **2016**, *28*, 5425–5446.

(8) Kang, T.-S.; Smith, A. P.; Taylor, B. E.; Durstock, M. F. Fabrication of Highly-Ordered TiO_2 Nanotube Arrays and Their Use in Dye-Sensitized Solar Cells. *Nano Letters* **2009**, *9*, 601–606.

(9) Kuang, D.; Brillet, J.; Chen, P.; Takata, M.; Uchida, S.; Miura, H.; Sumioka, K.; Zakeeruddin, S. M.; Grätzel, M. Application of Highly Ordered TiO_2 Nanotube Arrays in Flexible Dye-Sensitized Solar Cells. *ACS Nano* **2008**, *2*, 1113–1116.

(10) Fujishima, A.; Honda, K. Electrochemical Photolysis of Water at a Semiconductor Electrode. *Nature* **1972**, *238*, 37–38.

(11) Khan, S. U.; Al-Shahry, M.; Ingler, W. B. Efficient Photochemical Water Splitting by a Chemically Modified n-TiO_2. *Science* **2002**, *297*, 2243–2245.

(12) Ni, M.; Leung, M. K.; Leung, D. Y.; Sumathy, K. A Review and Recent Developments in Photocatalytic Water-Splitting Using TiO_2 for Hydrogen Production. *Renewable and Sustainable Energy Reviews* **2007**, *11*, 401–425.

(13) Esterkin, C.; Negro, A.; Alfano, O.; Cassano, A. Air Pollution Remediation in a Fixed Bed Photocatalytic Reactor Coated with TiO_2. *AIChE Journal* **2005**, *51*, 2298–2310.

(14) Antonello, A.; Soliveri, G.; Meroni, D.; Cappelletti, G.; Ardizzone, S. Photocatalytic Remediation of Indoor Pollution by Transparent TiO_2 Films. *Catalysis Today* **2014**, *230*, 35–40.

(15) Rhatigan, S.; Nolan, M. CO_2 and Water Activation on Ceria Nanocluster Modified TiO_2 Rutile (110). *Journal of Materials Chemistry A* **2018**, *6*, 9139–9152.

(16) Fronzi, M.; Daly, W.; Nolan, M. Reactivity of Metal Oxide Nanocluster Modified Rutile and Anatase TiO_2: Oxygen Vacancy Formation and CO_2 Interaction. *Applied Catalysis A: General* **2016**, *521*, 240 – 249.

(17) Yu, J.; Low, J.; Xiao, W.; Zhou, P.; Jaroniec, M. Enhanced Photocatalytic CO_2-Reduction Activity of Anatase TiO_2 by Coexposed {001} and {101} Facets. *Journal of the American Chemical Society* **2014**, *136*, 8839–8842.

(18) Reddy, K. M.; Manorama, S. V.; Reddy, A. R. Bandgap Studies on Anatase Titanium Dioxide Nanoparticles. *Materials Chemistry and Physics* **2003**, *78*, 239 – 245.

(19) Sankapal, B.; Lux-Steiner, M.; Ennaoui, A. Synthesis and Characterization of Anatase-TiO_2 Thin Films. *Applied Surface Science* **2005**, *239*, 165 – 170.

(20) Tang, H.; Prasad, K.; Sanjinés, R.; Schmid, P. E.; Lévy, F. Electrical and Optical

Properties of TiO_2 Anatase Thin Films. *Journal of Applied Physics* **1994**, *75*, 2042–2047.

(21) Fahmi, A.; Minot, C.; Silvi, B.; Causá, M. Theoretical Analysis of the Structures of Titanium Dioxide Crystals. *Physical Review B* **1993**, *47*, 11717–11724.

(22) Fox, M. A.; Dulay, M. T. Heterogeneous Photocatalysis. *Chemical Reviews* **1993**, *93*, 341–357.

(23) Linsebigler, A. L.; Lu, G.; Yates, J. T. Photocatalysis on TiO_2 Surfaces: Principles, Mechanisms, and Selected Results. *Chemical Reviews* **1995**, *95*, 735–758.

(24) Naicker, P. K.; Cummings, P. T.; Zhang, H.; Banfield, J. F. Characterization of Titanium Dioxide Nanoparticles Using Molecular Dynamics Simulations. *The Journal of Physical Chemistry B* **2005**, *109*, 15243–15249.

(25) Liu, G.; Sun, C.; Yang, H. G.; Smith, S. C.; Wang, L.; Lu, G. Q.; Cheng, H.-M. Nanosized Anatase TiO_2 Single Crystals for Enhanced Photocatalytic Activity. *Chemical Communications* **2010**, *46*, 755–757.

(26) Roy, N.; Sohn, Y.; Pradhan, D. Synergy of Low Energy {101} and High Energy {001} TiO_2 Crystal Facets for Enhanced Photocatalysis. *ACS Nano* **2013**, *7*, 2532–2540.

(27) Dinh, C.-T.; Nguyen, T.-D.; Kleitz, F.; Do, T.-O. Shape Controlled Synthesis of Highly Crystalline Titania Nanocrystals. *ACS Nano* **2009**, *3*, 3737–3743.

(28) Fang, W. Q.; Gong, X.-Q.; Yang, H. G. On the Unusual Properties of Anatase TiO_2 Exposed by Highly Reactive Facets. *The Journal of Physical Chemistry Letters* **2011**, *2*, 725–734.

(29) Murakami, N.; Kurihara, Y.; Tsubota, T.; Ohno, T. Shape-Controlled Anatase Titanium(IV) Oxide Particles Prepared by Hydrothermal Treatment of Peroxo Titanic

Acid in the Presence of Polyvinyl Alcohol. *The Journal of Physical Chemistry C* **2009**, *113*, 3062–3069.

(30) Maitani, M. M.; Tanaka, K.; Mochizuki, D.; Wada, Y. Enhancement of Photoexcited Charge Transfer by {001} Facet-Dominating TiO_2 Nanoparticles. *The Journal of Physical Chemistry Letters* **2011**, *2*, 2655–2659.

(31) Chang, L.; Xiguang, H.; Shuifen, X.; Qin, K.; Xue, W.; Mingshang, J.; Zhaoxiong, X.; Lansun, Z. Enhancing the Photocatalytic Activity of Anatase TiO_2 by Improving the Specific Facet-Induced Spontaneous Separation of Photogenerated Electrons and Holes. *Chemistry An Asian Journal* **2012**, *8*, 282–289.

(32) Wang, Q.; Zhang, Z.; Zakeeruddin, S. M.; Grätzel, M. Enhancement of the Performance of Dye-Sensitized Solar Cell by Formation of Shallow Transport Levels Under Visible Light Illumination. *The Journal of Physical Chemistry C* **2008**, *112*, 7084–7092.

(33) Weidmann, J.; Dittrich, T.; Konstantinova, E.; Lauermann, I.; Uhlendorf, I.; Koch, F. Influence of Oxygen and Water Related Surface Defects on the Dye Sensitized TiO_2 Solar Cell. *Solar Energy Materials and Solar Cells* **1999**, *56*, 153–165.

(34) Bailes, M.; Cameron, P.; Lobato, K.; Peter, L. Determination of the Density and Energetic Distribution of Electron Traps in Dye-Sensitized Nanocrystalline Solar Cells. *The Journal of Physical Chemistry B* **2005**, *109*, 15429–15435.

(35) Dimitrijevic, N. M.; Saponjic, Z. V.; Rabatic, B. M.; Poluektov, O. G.; Rajh, T. Effect of Size and Shape of Nanocrystalline TiO_2 on Photogenerated Charges. An EPR Study. *The Journal of Physical Chemistry C* **2007**, *111*, 14597–14601.

(36) Skinner, D. E.; Colombo Jr, D. P.; Cavaleri, J. J.; Bowman, R. M. Femtosecond Investigation of Electron Trapping in Semiconductor Nanoclusters. *The Journal of Physical Chemistry* **1995**, *99*, 7853–7856.

(37) Mercado, C. C.; Knorr, F. J.; McHale, J. L.; Usmani, S. M.; Ichimura, A. S.; Saraf, L. V. Location of Hole and Electron Traps on Nanocrystalline Anatase TiO_2. *The Journal of Physical Chemistry C* **2012**, *116*, 10796–10804.

(38) Papageorgiou, A. C.; Beglitis, N. S.; Pang, C. L.; Teobaldi, G.; Cabailh, G.; Chen, Q.; Fisher, A. J.; Hofer, W. A.; Thornton, G. Electron Traps and Their Effect on the Surface Chemistry of TiO_2 (110). *Proceedings of the National Academy of Sciences* **2010**, *107*, 2391–2396.

(39) Mora-Seró, I.; Bisquert, J. Fermi Level of Surface States in TiO_2 Nanoparticles. *Nano Letters* **2003**, *3*, 945–949.

(40) Szczepankiewicz, S. H.; Moss, J. A.; Hoffmann, M. R. Electron Traps and the Stark Effect on Hydroxylated Titania Photocatalysts. *The Journal of Physical Chemistry B* **2002**, *106*, 7654–7658.

(41) Howe, R. F.; Gratzel, M. EPR Observation of Trapped Electrons in Colloidal Titanium Dioxide. *The Journal of Physical Chemistry* **1985**, *89*, 4495–4499.

(42) Thomas, A. G.; Flavell, W. R.; Kumarasinghe, A. R.; Mallick, A. K.; Tsoutsou, D.; Smith, G. C.; Stockbauer, R.; Patel, S.; Grätzel, M.; Hengerer, R. Resonant photoemission of anatase TiO_2 (101) and (001) single crystals. *Physical Review B* **2003**, *67*, 035110.

(43) Elmaslmane, A. R.; Watkins, M. B.; McKenna, K. P. First-Principles Modeling of Polaron Formation in TiO_2 Polymorphs. *Journal of Chemical Theory and Computation* **2018**, *14*, 37403751.

(44) Carey, J. J.; McKenna, K. P. Does Polaronic Self-Trapping Occur at Anatase TiO_2 Surfaces? *The Journal of Physical Chemistry C* **2018**, *122*, 27540–27553.

(45) Setvin, M.; Franchini, C.; Hao, X.; Schmid, M.; Janotti, A.; Kaltak, M.; Van de Walle, C. G.; Kresse, G.; Diebold, U. Direct View at Excess Electrons in TiO_2 Rutile and Anatase. *Physical Review Letters* **2014**, *113*, 086402.

(46) Deskins, N. A.; Dupuis, M. Electron Transport via Polaron Hopping in Bulk TiO_2: A Density Functional Theory Characterization. *Physical Review B* **2007**, *75*, 195212.

(47) Deskins, N. A.; Dupuis, M. Intrinsic Hole Migration Rates in TiO_2 from Density Functional Theory. *The Journal of Physical Chemistry C* **2009**, *113*, 346–358.

(48) Deskins, N. A.; Rousseau, R.; Dupuis, M. Localized Electronic States from Surface Hydroxyls and Polarons in TiO_2 (110). *The Journal of Physical Chemistry C* **2009**, *113*, 14583–14586.

(49) Morgan, B. J.; Scanlon, D. O.; Watson, G. W. Small Polarons in Nb- and Ta- Doped Rutile and Anatase TiO_2. *Journal of Materials Chemistry* **2009**, *19*, 5175–5178.

(50) Morgan, B. J.; Watson, G. W. Polaronic Trapping of Electrons and Holes by Native Defects in Anatase TiO_2. *Physical Review B* **2009**, *80*, 233102.

(51) Diebold, U.; Ruzycki, N.; Herman, G. S.; Selloni, A. One Step Towards Bridging the Materials gap: Surface Studies of TiO_2 Anatase. *Catalysis Today* **2003**, *85*, 93–100.

(52) Xue-Qing Gong, M. B., Annabella Selloni; Diebold, U. Steps on anatase TiO_2 (101). *Nature Materials* **2006**, *5*, 665670.

(53) Liang, Y.; Gan, S.; Chambers, S. A.; Altman, E. I. Surface Structure of Anatase TiO_2(001) : Reconstruction, Atomic Steps, and Domains. *Physical Review B* **2001**, *63*, 235402.

(54) Gong, X.-Q.; Selloni, A.; Dulub, O.; Jacobson, P.; Diebold, U. Small Au and Pt Clusters at the Anatase TiO_2 (101) Surface: Behavior at Terraces, Steps, and Surface Oxygen Vacancies. *Journal of the American Chemical Society* **2008**, *130*, 370–381.

(55) Di Valentin, C.; Selloni, A. Bulk and Surface Polarons in Photoexcited Anatase TiO_2. *The Journal of Physical Chemistry Letters* **2011**, *2*, 2223–2228.

(56) Finazzi, E.; Di Valentin, C.; Pacchioni, G.; Selloni, A. Excess Electron States in Reduced Bulk Anatase TiO_2: Comparison of Standard GGA, GGA+U, and Hybrid DFT Calculations. *The Journal of Chemical Physics* **2008**, *129*, 154113.

(57) Cheng, H.; Selloni, A. Surface and Subsurface Oxygen Vacancies in Anatase TiO_2 and Differences with Rutile. *Physical Review B* **2009**, *79*, 092101.

(58) Mattioli, G.; Filippone, F.; Alippi, P.; Bonapasta, A. A. *Ab-initio* Study of the Electronic States Induced by Oxygen Vacancies in Rutile and Anatase TiO_2. *Physical Review B* **2008**, *78*, 241201.

(59) Di Valentin, C.; Pacchioni, G.; Selloni, A.; Livraghi, S.; Giamello, E. Characterization of Paramagnetic Species in N-doped TiO_2 Powders by EPR Spectroscopy and DFT Calculations. *The Journal of Physical Chemistry B* **2005**, *109*, 11414–11419.

(60) Di Valentin, C.; Finazzi, E.; Pacchioni, G.; Selloni, A.; Livraghi, S.; Paganini, M. C.; Giamello, E. N-doped TiO_2: Theory and Experiment. *Chemical Physics* **2007**, *339*, 44–56.

(61) Nakamura, R.; Tanaka, T.; Nakato, Y. Mechanism for Visible Light Responses in Anodic Photocurrents at N-doped TiO_2 Film Electrodes. *The Journal of Physical Chemistry B* **2004**, *108*, 10617–10620.

(62) Tokudome, H.; Miyauchi, M. N-doped TiO_2 Nanotube with Visible Light Activity. *Chemistry Letters* **2004**, *33*, 1108–1109.

(63) Lin, Z.; Orlov, A.; Lambert, R. M.; Payne, M. C. New Insights into the Origin of Visible Light Photocatalytic Activity of Nitrogen-Doped and Oxygen-Deficient Anatase TiO2. *The Journal of Physical Chemistry B* **2005**, *109*, 20948–20952, PMID: 16853715.

(64) Zhang, R.; Wang, Q.; Liang, J.; Li, Q.; Dai, J.; Li, W. Optical Properties of N and Transition Metal R (R=V, Cr, Mn, Fe, Co, Ni, Cu, and Zn) Co-doped Anatase TiO_2. *Physica B: Condensed Matter* **2012**, *407*, 2709 – 2715.

(65) Peng, H.; Li, J.; Li, S.-S.; Xia, J.-B. First-principles Study of the Electronic Structures and Magnetic Properties of $3d$ Transition Metal-doped Anatase TiO_2. *Journal of Physics: Condensed Matter* **2008**, *20*, 125207.

(66) Tian,; Liu, DFT Description on Electronic Structure and Optical Absorption Properties of Anionic S-Doped Anatase TiO_2. *The Journal of Physical Chemistry B* **2006**, *110*, 17866–17871.

(67) Tian, G.; Pan, K.; Fu, H.; Jing, L.; Zhou, W. Enhanced Photocatalytic Activity of S-doped TiO_2/ZrO_2 Nanoparticles Under Visible-light Irradiation. *Journal of Hazardous Materials* **2009**, *166*, 939 – 944.

(68) Umebayashi, T.; Yamaki, T.; Itoh, H.; Asai, K. Band Gap Narrowing of Titanium Dioxide by Sulfur Doping. *Applied Physics Letters* **2002**, *81*, 454–456.

(69) Di Valentin, C.; Pacchioni, G.; Selloni, A. Theory of Carbon Doping of Titanium Dioxide. *Chemistry of Materials* **2005**, *17*, 6656–6665.

(70) Wang, H.; Lewis, J. P. Effects of Dopant States on Photoactivity in Carbon-doped TiO_2. *Journal of Physics: Condensed Matter* **2005**, *17*, L209–L213.

(71) In, S.; Orlov, A.; Berg, R.; Garca, F.; Pedrosa-Jimenez, S.; Tikhov, M. S.; Wright, D. S.; Lambert, R. M. Effective Visible Light-Activated B-Doped and B,N-Codoped TiO_2 Photocatalysts. *Journal of the American Chemical Society* **2007**, *129*, 13790–13791.

(72) Zhao, Z.; Liu, Q. Effects of Lanthanide Doping on Electronic Structures and Optical

Properties of Anatase TiO_2 From Density Functional Theory Calculations. *Journal of Physics D: Applied Physics* **2008**, *41*, 085417.

(73) Lippens, P. E.; Chadwick, A. V.; Weibel, A.; Bouchet, R.; Knauth, P. Structure and Chemical Bonding in Zr-Doped Anatase TiO2 Nanocrystals. *The Journal of Physical Chemistry C* **2008**, *112*, 43–47.

(74) Venkatachalam, N.; Palanichamy, M.; Arabindoo, B.; Murugesan, V. Enhanced Photocatalytic Degradation of 4-chlorophenol by Zr^{4+} Doped Nano TiO_2. *Journal of Molecular Catalysis A: Chemical* **2007**, *266*, 158 – 165.

(75) Shojaie, A. F.; Loghmani, M. H. La^{3+} and Zr^{4+} Co-doped Anatase Nano TiO_2 by Sol-microwave Method. *Chemical Engineering Journal* **2010**, *157*, 263 – 269.

(76) Yu, J. C.; Yu,; Ho,; Jiang,; Zhang, Effects of F- Doping on the Photocatalytic Activity and Microstructures of Nanocrystalline TiO_2 Powders. *Chemistry of Materials* **2002**, *14*, 3808–3816.

(77) Guidon, M.; Hutter, J.; VandeVondele, J. Robust Periodic HartreeFock Exchange for Large-Scale Simulations Using Gaussian Basis Sets. *Journal of Chemical Theory and Computation* **2009**, *5*, 3010–3021.

(78) VandeVondele, J.; Krack, M.; Mohamed, F.; Parrinello, M.; Chassaing, T.; Hutter, J. Quickstep: Fast and Accurate Density Functional Calculations Using a Mixed Gaussian and Plane Waves Approach. *Computer Physics Communications* **2005**, *167*, 103 – 128.

(79) VandeVondele, J.; Hutter, J. Gaussian Basis Sets for Accurate Calculations on Molecular Systems in Gas and Condensed Phases. *The Journal of Chemical Physics* **2007**, *127*, 114105.

(80) Goedecker, S.; Teter, M.; Hutter, J. Separable Sual-Space Gaussian Pseudopotentials. *Physical Review B* **1996**, *54*, 1703–1710.

(81) Hartwigsen, C.; Goedecker, S.; Hutter, J. Relativistic Separable Dual-Space Gaussian Pseudopotentials from H to Rn. *Physical Review B* **1998**, *58*, 3641–3662.

(82) Krack, M. Pseudopotentials for H to Kr Optimized for Gradient-Corrected Exchange-Correlation Functionals. *Theoretical Chemistry Accounts* **2005**, *114*, 145–152.

(83) Bader, R. F. Atoms in Molecules. *Accounts of Chemical Research* **1985**, *18*, 9–15.

(84) Henkelman, G.; Arnaldsson, A.; Jónsson, H. A Fast and Robust Algorithm for Bader Decomposition of Charge Density. *Computational Materials Science* **2006**, *36*, 354–360.

(85) Sanville, E.; Kenny, S. D.; Smith, R.; Henkelman, G. Improved Grid-based Algorithm for Bader Charge Allocation. *Journal of Computational Chemistry* **2007**, *28*, 899–908.

(86) Tang, W.; Sanville, E.; Henkelman, G. A Grid-based Bader Analysis Algorithm without Lattice Bias. *Journal of Physics: Condensed Matter* **2009**, *21*, 084204.

(87) Yu, M.; Trinkle, D. R. Accurate and Efficient Algorithm for Bader Charge Integration. *The Journal of Chemical Physics* **2011**, *134*, 064111.

(88) Momma, K.; Izumi, F. VESTA: a Three-dimensional Visualization System for Electronic and Structural Analysis. *Journal of Applied Crystallography* **2008**, *41*, 653–658.

(89) Momma, K.; Izumi, F. VESTA 3 for Three-dimensional Visualization of Crystal, volumetric and morphology data. *Journal of Applied Crystallography* **2011**, *44*, 1272–1276.

(90) Wolf, M. J.; McKenna, K. P.; Shluger, A. L. Hole Trapping at Surfaces of m-ZrO_2 and m-HfO_2 Nanocrystals. *The Journal of Physical Chemistry C* **2012**, *116*, 25888–25897.

(91) Stoneham, A.; Gavartin, J.; Shluger, A.; Kimmel, A.; Ramo, D. M.; Rønnow, H.; Aeppli, G.; Renner, C. Trapping, Self-trapping and the Polaron Family. *Journal of Physics: Condensed Matter* **2007**, *19*, 255208.

(92) Gavartin, J.; Muñoz Ramo, D.; Shluger, A.; Bersuker, G.; Lee, B. Negative Oxygen Vacancies in HfO_2 as Charge Traps in High-k Stacks. *Applied Physics Letters* **2006**, *89*, 082908.

(93) Shluger, A. L.; Mckenna, K. P.; Sushko, P. V.; Ramo, D. M.; Kimmel, A. Modelling of Electron and Hole Trapping in Oxides. *Modelling and Simulation in Materials Science and Engineering* **2009**, *17*, 084004.

(94) Allen, J. P.; Carey, J. J.; Walsh, A.; Scanlon, D. O.; Watson, G. W. Electronic Structures of Antimony Oxides. *The Journal of Physical Chemistry C* **2013**, *117*, 14759–14769.

(95) Egdell, R.; Flavell, W.; Tavener, P. Antimony-doped Tin (IV) Oxide: Surface Composition and Electronic Structure. *Journal of Solid State Chemistry* **1984**, *51*, 345–354.

(96) Mishra, K. C.; Johnson, K. H.; Schmidt, P. C. Electronic Structure of Antimony-doped Tin Oxide. *Physical Review B* **1995**, *51*, 13972–13976.

(97) Ye, J.; Liu, W.; Cai, J.; Chen, S.; Zhao, X.; Zhou, H.; Qi, L. Nanoporous Anatase TiO_2 Mesocrystals: Additive-free Synthesis, Remarkable Crystalline-phase Stability, and Improved Lithium Insertion Behavior. *Journal of the American Chemical Society* **2010**, *133*, 933–940.

(98) Krtil, P.; Fattakhova, D.; Kavan, L.; Burnside, S.; Grätzel, M. Lithium Insertion into Self-organized Mesoscopic TiO_2 (Anatase) Electrodes. *Solid State Ionics* **2000**, *135*, 101–106.

(99) Bessekhouad, Y.; Robert, D.; Weber, J.-V.; Chaoui, N. Effect of Alkaline-doped TiO_2 on photocatalytic efficiency. *Journal of Photochemistry and Photobiology A: Chemistry* **2004**, *167*, 49–57.

(100) Wagemaker, M.; Borghols, W. J.; Mulder, F. M. Large Impact of Particle Size on Insertion Reactions. A Case for Anatase Li_x TiO_2. *Journal of the American Chemical Society* **2007**, *129*, 4323–4327.

(101) Shi, L.; Li, C.; Gu, H.; Fang, D. Morphology and Properties of Ultrafine SnO_2–TiO_2 Coupled Semiconductor Particles. *Materials Chemistry and Physics* **2000**, *62*, 62–67.

(102) Shang, J.; Yao, W.; Zhu, Y.; Wu, N. Structure and Photocatalytic Performances of Glass/SnO_2/TiO_2 Interface Composite Film. *Applied Catalysis A: General* **2004**, *257*, 25–32.

(103) Gao, B.; Lim, T. M.; Subagio, D. P.; Lim, T.-T. Zr-doped TiO_2 for Enhanced Photocatalytic Degradation of Bisphenol A. *Applied Catalysis A: General* **2010**, *375*, 107–115.

(104) Wang, Y. M.; Liu, S. W.; Lü, M. K.; Wang, S. F.; Gu, F.; Gai, X. Z.; Cui, X. P.; Pan, J. Preparation and Photocatalytic Properties of Zr^{4+} -doped TiO_2 Nanocrystals. *Journal of Molecular Catalysis A: Chemical* **2004**, *215*, 137–142.

(105) Lippens, P.-E.; Chadwick, A. V.; Weibel, A.; Bouchet, R.; Knauth, P. Structure and Chemical Bonding in Zr-doped Anatase TiO_2 Nanocrystals. *The Journal of Physical Chemistry C* **2008**, *112*, 43–47.

(106) Iwaszuk, A.; Nolan, M. Electronic Structure and Reactivity of Ce-and Zr-doped TiO_2: Assessing the Reliability of Density Functional Theory Approaches. *The Journal of Physical Chemistry C* **2011**, *115*, 12995–13007.

Graphical TOC Entry